Probing heavy dark matter in red giants

Sougata Ganguly,[1,*] Minxi He,[1,†] Chang Sub Shin,[2,1,3,‡] Oscar Straniero,[4,5,§] and Seokhoon Yun[6,1,‖]

[1]*Particle Theory and Cosmology Group, Center for Theoretical Physics of the Universe, Institute for Basic Science (IBS), Daejeon 34126, Republic of Korea*

[2]*Department of Physics and Institute for Sciences of the Universe, Chungnam National University, Daejeon 34134, Republic of Korea*

[3]*School of Physics, Korea Institute for Advanced Study, Seoul 02455, Republic of Korea*

[4]*INAF, Osservatorio Astronomico d'Abruzzo, 64100 Teramo, Italy*

[5]*Istituto Nazionale di Fisica Nucleare-Sezione di Roma, Piazzale Aldo Moro 2, 00185 Roma, Italy*

[6]*Department of Physics, Kyungpook National University, Daegu 41566, Republic of Korea*

(Received 11 September 2025; accepted 3 April 2026; published 27 April 2026)

Red giants (RGs) provide a promising astrophysical environment for capturing dark matter (DM) via elastic scattering with stellar nuclei. Captured DM particles migrate toward the helium-rich core and accumulate into a compact configuration. As the DM population grows, it can become self-gravitating and undergo gravitational collapse, leading to adiabatic contraction through interactions with the ambient medium. The resulting energy release, through elastic scattering and, where relevant, DM annihilation during collapse, locally heats the stellar core and can trigger helium ignition earlier than that predicted by standard stellar evolution. We analyze the conditions under which DM-induced heating leads to runaway helium burning and identify the critical DM mass required for ignition. Imposing the observational constraint that helium ignition must not occur before the observed luminosity at the tip of the RG branch, we translate these conditions into bounds on DM properties. Remarkably, we find that RGs are sensitive to DM, particularly with masses around 10^{11} GeV and spin-independent scattering cross sections near 10^{-37} cm^2, which is comparable to the reach of current terrestrial direct detection experiments. Noteworthy, observations of RG stars provide a unique probe for high-mass and large-cross-section DM, a regime that remains currently inaccessible to direct detection experiments.

DOI: 10.1103/x43m-y414

I. INTRODUCTION

Dark matter (DM) constitutes approximately 27% of the present-day mass-energy content of the Universe, as supported by a wide range of cosmological and astrophysical observations, including the cosmic microwave background [1], Galactic rotation curves [2], and the Bullet Cluster [3]. Despite DM's gravitational influence being well established, the fundamental nature of DM remains elusive, largely due to its lack of significant interactions with ordinary matter beyond gravity [4].

In the standard Λ cold dark matter paradigm, DM is assumed to be cold and collisionless, successfully explaining large-scale structure formation and other gravitational phenomena. A well-studied candidate in this framework is the weakly interacting massive particle (WIMP), which is thermally produced in the early Universe with a weak scale mass and a weak interaction strength [5]. This scenario naturally accounts for the observed DM abundance, which makes it highly appealing from a theoretical perspective [6–8]. However, null results from direct detection experiments such as XENON1T [9] and Large Underground Xenon (LUX) [10] have excluded much of the WIMP parameter space. For instance, spin-independent cross sections larger than $\sim 10^{-46}$ cm^2 are ruled out for WIMP masses between 5 and 100 GeV, well beyond what is required by relic abundance considerations.

These constraints have renewed interest in heavy dark matter (HDM) scenarios, where the DM mass lies well above the weak scale. The number of recoil events in direct detection experiments decreases with increasing DM mass, which allows HDM to evade current bounds. However, HDM is typically incompatible with thermal production,

*Contact author: sganguly0205@ibs.re.kr
†Contact author: heminxi@ibs.re.kr
‡Contact author: csshin@cnu.ac.kr
§Contact author: oscar.straniero@inaf.it
‖Contact author: seokhoon.yun@knu.ac.kr

Published by the American Physical Society under the terms of the Creative Commons Attribution 4.0 International license. Further distribution of this work must maintain attribution to the author(s) and the published article's title, journal citation, and DOI. Funded by SCOAP³.

as unitarity bounds on annihilation cross sections limit the mass of thermally produced DM to below ∼100 TeV [11]. Instead, the correct HDM relic abundance can be achieved through various mechanisms involving sizable interactions with the Standard Model (SM) plasma [12–23]. These interactions may also lead to observable consequences in current or future experiments.

Beyond laboratory searches, stellar environments offer a promising avenue to probe DM interactions with the visible sector governed by the SM [24]. Many studies have demonstrated that stars can constrain DM models through capture [25,26] and then energy transport [27–31] or heating effects, with the sensitivity depending on stellar structure and evolutionary stage. Also, DM accumulation can affect the inner structures of main sequence stars, which can constrain asymmetric DM [32–35]. Among these, red giants (RGs) are particularly interesting due to the high densities and temperatures in their helium-rich cores.

During the main sequence, hydrogen fusion in the stellar core gradually builds up an innermost region composed almost entirely of helium. Since helium fusion requires significantly higher densities and temperatures, the helium core cannot burn its fuel and remains inert. As the helium core contracts under gravity, the surrounding shell of hydrogen around the core becomes hotter and denser to ignite hydrogen burning at an increasingly rapid rate. The resulting outward pressure causes the stellar envelope to expand and cool to make the star redder and more luminous as a transition into the RG branch (RGB) on the Hertzsprung-Russell (HR) diagram. Driven by hydrogen burning, the helium-rich core grows in mass, so that its density and temperature increase and electron degeneracy develops. Once the core temperature reaches approximately 10^8 K, a thermonuclear runaway occurs through the triple-α process: ${}^4_2\mathrm{He} + {}^4_2\mathrm{He} \rightarrow {}^8_4\mathrm{Be} + \gamma$, followed by ${}^8_4\mathrm{Be} + {}^4_2\mathrm{He} \rightarrow {}^{12}_6\mathrm{C} + \gamma$. This violent event, known as the helium flash, releases enough energy to lift the degeneracy of the core, halting the runaway and leading to a stable phase of core helium burning. The star subsequently settles onto the horizontal branch in the HR diagram. In standard stellar evolution, the core mass at the moment of helium ignition is a robust and well-predicted quantity. Indeed, current stellar evolution models yield tip of the red-giant branch (TRGB) luminosities that closely match available observations [36]. Hence, any deviations from this prediction, such as premature (or delayed) helium flash induced by an extra heating [37–39] (or cooling [24,40–42]) mechanism, can leave observable imprints on stellar populations, especially in globular clusters.

In this work, we investigate the capture of DM particles by RG cores and their potential impact on stellar evolution, particularly on the timing of helium ignition. The schematic overview is illustrated in Fig. 1. DM particles lose kinetic energy through repeated elastic scatterings with nuclei in the stellar interior and become gravitationally bound once their velocity falls below the escape speed. As they continue to lose energy, their orbits shrink deeper into the core; we refer to this process as "ingress." Eventually, the captured DM population thermalizes with the stellar medium, forming a compact DM sphere at the stellar center. When the DM density within this sphere surpasses that of the surrounding stellar matter, its self-gravity dominates such that the gravitational collapse can occur. This collapse deposits DM energy into the ambient material through elastic scattering and/or annihilation, depending on the underlying interaction model. In particular, for HDM, since the pair-annihilation cross section is intrinsically small due to the unitarity bound, DM particles can accumulate to extremely high densities without being efficiently depleted by annihilation. We highlight that this delayed annihilation can therefore provide a concentrated and intense source of heating at the stellar center.

If this exotic heating exceeds the rate of thermal diffusion, it can ignite a local helium flame that propagates outward through the core, driving a runaway helium ignition. This scenario stands in sharp contrast to standard stellar evolution, where efficient neutrino cooling via the plasmon decay suppresses central ignition and instead

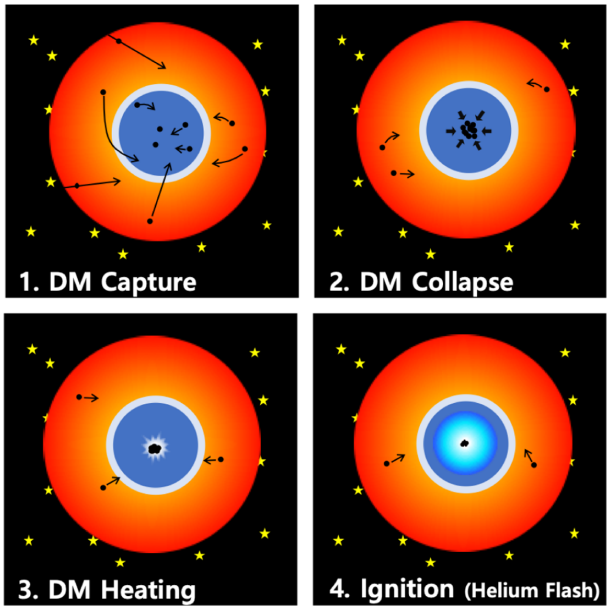


FIG. 1. Schematic overview of the main phases of DM capture and its impact on RG evolution, proceeding in order as follows. Upper left: DM particles are captured via elastic scatterings with nuclei (Sec. II A). Upper right: captured DM concentrates near the stellar center through ingress (Sec. II B) and subsequently thermalizes (Sec. II C). Once the DM density exceeds that of the ambient medium, the DM core gravitationally collapses (Sec. II D). Lower left: the collapsed DM core heats the surrounding medium. If the heating overcomes diffusive cooling, it can trigger helium ignition (Sec. III A). Lower right: runaway helium burning occurs when DM heating satisfies the trigger mass condition (Sec. III B).

causes helium burning to commence in an off-center shell of the degenerate core. In our case, dynamical DM heating shifts the ignition site to the stellar center, because the DM heating can increase the temperature of the ignition site to a temperature higher than 10^8 K, where the nuclear reaction rate dominates over the plasmon decay rate. To quantify this process, we estimate the minimum amount of core material that must be heated to ignite helium and initiate this runaway fusion, namely the trigger mass for helium flash [43,44].

A premature, DM-induced helium flash leads to a smaller helium core mass than in standard stellar evolution, resulting in a lower luminosity at the TRGB. By requiring consistency with observed RG populations, we derive stringent constraints on the DM-nucleon scattering cross section.

The remainder of the paper is organized as follows: in Sec. II, we discuss the dynamics of DM particles captured by a star, including their concentration at the center through elastic scattering with the stellar medium. Section III explores how a sufficiently dense and self-gravitating DM core can deposit energy into the surrounding material via elastic scatterings and/or annihilation and potentially trigger helium ignition in RGs. We provide an estimate of the trigger mass required for such a runaway process. Finally, we conclude with a summary of our main findings. In the Appendixes, we provide useful formulas and expressions for our analysis. For the sake of convenience, we adopt $\hbar = c = k_B = 1$.

II. DARK MATTER CAPTURE IN STARS

In this section, we discuss the capture of DM particles (χ) by a star and their subsequent concentration in the innermost region. We divide the process into distinct phases: capture, ingress, thermalization, and gravitational collapse. Throughout these stages, we assume that the dynamics are governed by elastic scatterings between DM and nuclei, as the DM number density is too low for the DM annihilation to significantly affect the system. The conditions under which DM annihilation becomes relevant will be addressed in the next section.

DM particles originating from the galactic halos and located far away from a star can be gravitationally attracted by the star. The differential incoming DM flux can be written as [45,46]

$$d\mathcal{F}_\chi = \pi \frac{f(u)}{u}\, du\, dJ^2, \tag{1}$$

where $J = \omega(r) r \sin\theta$ is associated with the conserved angular momentum of a DM particle at radius r, $\omega(r) = \sqrt{v_e(r)^2 + u^2}$ is the speed of a DM particle at r with the local escape velocity $v_e(r)$ and the initial velocity at infinity, and θ is the angle between the DM velocity and the radial vector. The function $f(u)$ denotes the DM velocity distribution at infinity, which we assume to follow a Maxwell-Boltzmann distribution throughout our analysis, as follows:

$$f(u) = 3\sqrt{\frac{6}{\pi}} \frac{\rho_\chi u^2}{m_\chi \bar{v}^3} \exp\left(-\frac{3u^2}{2\bar{v}^2}\right), \tag{2}$$

where m_χ is the DM mass. For numerical analysis, we take the local DM density of $\rho_\chi = 0.3$ GeV/cm^3 and the averaged DM speed of $\bar{v} = 220$ km/s. Although the DM density in globular clusters is subject to significant uncertainties [47–56], our capture results scale linearly with the assumed density, making our conclusions robust to such variations.

In the presence of nongravitational interaction between DM and nuclei, DM particles can undergo elastic scattering with the stellar medium as they traverse the star. If the kinetic energy of a DM particle significantly exceeds that of target nuclei (typically set by temperature), the fractional kinetic energy loss per collision with a target nucleus T in the process $\chi + T \to \chi + T$ is given by

$$\frac{\Delta K_\chi}{K_\chi} = -\frac{4 m_\chi m_T}{(m_\chi + m_T)^2} x, \tag{3}$$

where K_χ denotes the kinetic energy of the incident DM, m_T is the mass of the target nucleus, and $x \in [0, 1]$ is a random variable associated with the scattering angle in the c.m. frame. For convenience, we define

$$\beta = \frac{4 m_\chi m_T}{(m_\chi + m_T)^2}, \tag{4}$$

which characterizes the efficiency of energy loss per collision.

A. Capture

A DM particle is captured by a star when it loses more energy through scattering than its initial kinetic energy at infinity, i.e., $m_\chi u^2/2$, during its passage through the stellar interior.

Given the fractional kinetic energy loss per collision described in Eq. (3), the probability that a DM particle with incoming kinetic energy $m_\chi \omega^2/2$ is captured after undergoing N scatterings is given by

$$g_N(\omega) = \left[\prod_{i=1}^{N} \int_0^1 dx_i\, f(x_i)\right] \Theta\left(\frac{v_e^2}{\omega^2} - \prod_{i=1}^{N} (1 - \beta x_i)\right), \tag{5}$$

where $f(x_i)$ is the probability density function (PDF) associated with the angular variable x_i for the ith scattering. For simplicity, we assume that each PDF is uniformly distributed and that scatterings are independent. In Appendix A, we derive an analytic approximation of

$g_N(\omega)$ in the limits of $N \gg 1$ and $\beta \ll 1$ (equivalently $m_\chi \gg m_T$), where the linear expansion of the step function argument is allowed.

The trajectory of a DM particle within the star is determined by its conserved angular momentum J. Since the escape velocity around the RG core ($\sim 0.01c$) exceeds the typical DM halo velocity ($\sim 10^{-3}c$), the DM path relies on θ, defined as the relative angle between the DM velocity and the radial direction. We define the core radius R_c as the radius at which the escape velocity is $\sqrt{2/3}$ times the escape velocity at the center. This $\sqrt{2/3}$ criterion corresponds to the escape velocity ratio for a uniformly dense sphere and aligns well with the straight-line approximation of particle trajectories.

Assuming a spherically symmetric stellar profile and adopting the straight-line approximation, the expected number of scatterings during the transit of DM through the star is given by the optical depth as follows:

$$\tau(y) = 2\int_0^{R_c y} n_T(r)\sigma_\chi T d\ell, \tag{6}$$

where $y \equiv \cos\theta$, n_T is the number density of target nuclei, and $r = \sqrt{R_c^2 + \ell^2 - 2R_c\ell y}$ is the radial distance along the path. Here, $\sigma_{\chi T}$ denotes the elastic scattering cross section between DM and target nuclei.

For momentum transfer scales below the typical inverse nucleon size (~ 10 fm ~ 0.1 MeV^{-1}), DM scatters coherently off the nucleons in a nucleus. At higher momentum transfers, such a coherence is lost and the cross section becomes suppressed. For heavy DM with $m_\chi \gg m_T$, this transition occurs at incident velocities around $v_\chi \sim 0.01c$. We parametrize $\sigma_{\chi T}$ in terms of the DM-nucleon elastic scattering cross section $\sigma_{\chi N}$, which is assumed to be spin-independent, isospin symmetric, and velocity independent, as follows:

$$\sigma_{\chi T} \simeq \sigma_{\chi N} A^2 \left(\frac{\mu_{\chi T}}{\mu_{\chi N}}\right)^2 F^2(E_R), \tag{7}$$

where A denotes the atomic mass number of the target nucleus, $\mu_{\chi T}$ ($\approx A\mu_{\chi N}$ for $m_\chi \gg m_T$) is the DM-nucleus reduced mass, and $F(E_R)$ is the nuclear form factor correction in terms of the recoil energy E_R [57]. This form factor is of order unity for $E_R \lesssim 1$ MeV and becomes suppressed for higher recoil energies.

Considering that each infinitesimal segment along the path contributes equally to the total optical depth, the probability for the N number of scatterings with the given optical depth in Eq. (6) follows the Poisson distribution function

$$p_N(y) = \frac{\tau(y)^N}{N!} e^{-\tau(y)}. \tag{8}$$

The DM capture rate can be expressed as [45]

$$\begin{aligned}\dot{\mathcal{C}} &= \int d\mathcal{F}_\chi \left(\sum_N g_N p_N\right)\Theta(\omega R_c - J) \\ &= \frac{3\pi R_c^2}{\bar{v}^3}\sqrt{\frac{6}{\pi}}\frac{\rho_\chi}{m_\chi}\int_0^\infty du\, u\, \omega^2 \exp\left(-\frac{3u^2}{2\bar{v}^2}\right) \\ &\quad \times \sum_{N=1}^{\infty} g_N \left(2\int_0^1 dy\, y\, p_N\right).\end{aligned} \tag{9}$$

Here, we take the escape velocity at the core radius, $v_e = v_e(R_c)$, based on the $\sqrt{2/3}$ criterion discussed above, which offers a conservative estimate under the straight-line approximation. In the remainder of this work, we adopt the escape velocity defined at the core radius.

Assuming a homogeneous density n_T, the capture rate scales linearly with $\sigma_{\chi T}$ in the small cross section regime, $\sigma_{\chi T} \ll (1/\beta n_T R_c)(\bar{v}^2/v_e^2)$. This behavior arises because DM particles with low initial velocities, $u^2 \lesssim (2v_e^2/3)(\beta n_T R_c)\sigma_{\chi T} \ll \bar{v}^2$, are more likely to be captured through a typical number of scatterings (i.e., the total optical depth τ). As a result, the capture probability becomes proportional to the optical depth and thus scales linearly with the cross section.

Conversely, when the cross section exceeds a critical value, $\sigma_{\chi T} \gtrsim (1/\beta n_T R_c)(\bar{v}^2/v_e^2)$, most incoming DM particles undergo sufficient scatterings to be captured. In this saturation regime, the capture rate reaches the geometric limit and becomes effectively independent of $\sigma_{\chi T}$.

We find that the analytic approximation for the capture rate provides a good fit to the full numerical results

$$\dot{\mathcal{C}} \simeq \dot{\mathcal{C}}_{\rm geo} \times \begin{cases} \left(\frac{\sigma_{\chi T}}{\sigma_{\rm thr}}\right) & \text{for } \sigma_{\chi T} \ll \sigma_{\rm thr} \\ 1 & \text{for } \sigma_{\chi T} > \sigma_{\rm thr} \end{cases}, \tag{10}$$

where the capture rate in the geometric limit is given by

$$\dot{\mathcal{C}}_{\rm geo} \equiv \pi R_c^2 \frac{\rho_\chi}{m_\chi}\bar{v}\sqrt{\frac{6}{\pi}}\left(\frac{v_e^2}{\bar{v}^2}\right), \tag{11}$$

and the threshold cross section is defined as

$$\sigma_{\rm thr} \equiv \frac{2}{\beta n_T R_c}\left(\frac{\bar{v}^2}{v_e^2}\right). \tag{12}$$

In realistic stellar environments, the interior medium typically consists of multiple nuclear species. This multiple species case can be appropriately addressed by generalizing the quantities for the fractional kinetic energy loss β and the optical depth τ as follows:

$$\beta = \frac{1}{\sum_i n_i \sigma_{\chi i}} \sum_i n_i \sigma_{\chi i} \frac{4 m_\chi m_i}{(m_\chi + m_i)^2}, \tag{13}$$

$$\tau(y) = \sum_i 2 \int_0^{R_c y} n_i(r) \sigma_{\chi i} d\ell, \tag{14}$$

where n_i is the number density of nuclei of species i, and $\sigma_{\chi i}$ is the corresponding DM-nucleus scattering cross section.

Finally, the total number of DM particles captured over the stellar lifetime can be obtained by integrating the time-dependent capture rate

$$N_\chi(t) = \int \dot{C}(t') dt'. \tag{15}$$

B. Ingress

Captured DM particles are gravitationally bound to the star, but typically follow elliptic orbits that remain mostly outside the stellar radius. Assuming the usual case of high orbital eccentricity, the total energy of a DM particle is approximately $E_\chi = -G M_c m_\chi / b$ where M_c is the stellar core mass, and b denotes the "apastron" distance (i.e., the farthest point from the stellar center). While a DM particle is inside the star ($r < R_c$), its kinetic energy is given by

$$K_\chi(r) = E_\chi - V_\chi(r) = E_\chi + \frac{G M_c m_\chi}{2 R_c^3} (3 R_c^2 - r^2). \tag{16}$$

Considering the averaged fractional energy loss for each collision given by $\beta/2$ and the orbital period of $2\pi (b/2)^{3/2} / \sqrt{G M_c}$, the DM energy loss rate can be estimated as

$$\frac{dE_\chi}{dt} = -\frac{\sqrt{2 G M_c}}{\pi b^{3/2}} \beta \int_0^{R_c} dr\, K_\chi(r) n_T(r) \sigma_{\chi T}. \tag{17}$$

Here, we approximate the evolution using a single representative DM trajectory that intersects the stellar radius. Using the relation $dE_\chi = (G M_c m_\chi / b^2) db$, Eq. (17) can be rewritten in terms of b as

$$\frac{db}{dt} = -\frac{\sqrt{2b}}{\pi \sqrt{G M_c} m_\chi} \beta \int_0^{R_c} dr\, K(r) n_T(r) \sigma_{\chi T}. \tag{18}$$

Under the assumption of a uniform stellar density, Eq. (18) simplifies to

$$\begin{aligned} \frac{db}{dt} &= -\frac{\sqrt{2b}}{\pi \sqrt{G M_c} m_\chi} \beta \frac{\tau_c}{2 R_c} \int_0^{R_c} dr\, K(r) \\ &= -\frac{\sqrt{G M_c} \beta \tau_c}{\sqrt{2} \pi R_c} \sqrt{b} \left(\frac{4}{3} - \frac{R_c}{b} \right), \end{aligned} \tag{19}$$

where $\tau_c \equiv \tau(1) \simeq 2 n_T \sigma_{\chi T} R_c$ represents the expected number of scatterings during a single crossing through the stellar core.

The average apastron distance of captured DMs, $\langle b \rangle$, relies on the DM-nucleus elastic scattering cross section, $\sigma_{\chi i}$. Given that each scattering reduces the energy by an average fraction $\beta/2$, and the total number of scatterings for a crossing over the stellar center is τ_c, the average energy of captured DMs is straightforwardly evaluated as $\langle E_\chi \rangle \approx -m_\chi \beta \tau_c v_e^2 / 4$. This yields an estimate for the average apastron distance as

$$\langle b \rangle \simeq \frac{2 R_c}{\beta \tau_c}. \tag{20}$$

The ingress phase ends when the DM orbit lies within the stellar core. The time scale for this inward migration can be estimated from Eq. (19) as[1]

$$\begin{aligned} t_{\rm ing} &\simeq \frac{3\pi R_c^{\frac{3}{2}}}{\sqrt{G M_c} \beta^{\frac{3}{2}} \tau_c^{\frac{3}{2}}} \\ &= 8.6\ {\rm Gyr}\, \rho_6^{-\frac{3}{2}} \left(\frac{M_c}{0.1 M_\odot} \right)^{-\frac{1}{2}} A^{-6} \\ &\quad \times \left(\frac{m_\chi}{10^{10}\ {\rm GeV}} \right)^{\frac{3}{2}} \left(\frac{\sigma_{\chi N}}{10^{-40}\ {\rm cm}^2} \right)^{-\frac{3}{2}}, \end{aligned} \tag{21}$$

assuming $\langle b \rangle \gg R_c$. In the final expression, we approximate $\sigma_{\chi T} \approx A^4 \sigma_{\chi N}$ and $m_T \simeq A m_N$, with the atomic number A. For notational convenience, we define the normalized variables

$$T_8 \equiv \frac{T_c}{10^8\ {\rm K}}, \qquad \rho_6 \equiv \frac{\rho_c}{10^6\ {\rm g/cm^3}}, \tag{22}$$

for the core temperature T_c and the core density ρ_c.

C. Thermalization

After the ingress phase, DM particles become fully confined within the stellar interior and undergo repeated collisions with the surrounding medium. The average fractional energy loss per elastic scattering with stellar nuclei is given by

$$\langle \Delta K_\chi \rangle = \frac{\beta}{2} \left(K_\chi - \frac{3}{2} T_c \right), \tag{23}$$

with the core temperature T_c. This expression shows that DM particles continue to lose energy until their kinetic

[1]This expression exhibits a different parametric dependence, particularly on the elastic scattering cross section $\sigma_{\chi i}$, compared to Ref. [46], due to a different assumption on the initial apastron distance.

energy becomes comparable to the thermal energy of the stellar medium, i.e., $K_\chi \sim \frac{3}{2}T_c$. Notably, in the high-energy limit where $K_\chi \gg T_c$ (e.g., the capture phase), this formula recovers the earlier description in Eq. (3).

The evolution of the DM kinetic energy is governed by the Boltzmann equation, as follows:

$$\frac{dK_\chi}{dt} = -n_T \sigma_{\chi T} v_{\rm rel} \frac{\beta}{2}\left(K_\chi - \frac{3}{2}T_c\right), \tag{24}$$

where the average relative velocity between DM and nuclei is approximately $v_{\rm rel} \approx \sqrt{2K_\chi/m_\chi + 3T_c/m_T}$. This equation indicates that the thermalization timescale $t_{\rm th}$ is sensitive to K_χ in the low-energy regime, particularly when the relative velocity is dominated by the thermal motion of nuclei, i.e., $v_{\rm rel} \approx \sqrt{3T_c/m_T}$. This results in

$$\begin{aligned} t_{\rm th} &\simeq \frac{2}{n_T \sigma_{\chi T}\beta}\sqrt{\frac{m_T}{3T_c}}\log\left[\frac{3m_\chi}{m_T}\right] \\ &= 1.8\times 10^{-5}\ {\rm Gyr}\,\rho_6^{-1}T_8^{-\frac{1}{2}}A^{-\frac{7}{2}} \\ &\quad\times\left(\frac{\sigma_{\chi N}}{10^{-40}\ {\rm cm}^2}\right)^{-1}\left(\frac{m_\chi}{10^{10}\ {\rm GeV}}\right)\log\left[\frac{3m_\chi}{m_T}\right]. \end{aligned} \tag{25}$$

Note that, formally, it takes an infinite time for the kinetic energy to reach exactly $K_\chi = 3T_c/2$ through scatterings. For practicality, we define thermalization as complete when the kinetic energy drops to $K_\chi = 2T_c$, which sufficiently ensures equilibrium with the stellar environment.

D. Gravitational collapse

Once thermalized, DM particles concentrate near the stellar core and settle into a compact configuration at the center. In the early stages, when the DM density remains low, the gravitational dynamics of the thermalized DM population are dominated by the background stellar potential. In this regime, considering the typical DM kinetic energy of $3T_c/2$, the virial theorem implies that the characteristic size of the thermalized DM sphere is

$$\begin{aligned} r_{\rm th} &= \sqrt{\frac{9T_c}{4\pi G\rho_{\rm c} m_\chi}} \\ &= 2.8\times 10^3\ {\rm cm}\left(\frac{m_\chi}{10^{10}\ {\rm GeV}}\right)^{-\frac{1}{2}}T_8^{\frac{1}{2}}\rho_6^{-\frac{1}{2}}. \end{aligned} \tag{26}$$

The total number of DM particles within the thermalized sphere continues to grow through continuous accumulation via the capture process, as described in Sec. II. Once the enclosed DM mass exceeds that of the ambient stellar material within the same radius, the configuration becomes self-gravitating. The threshold mass for the onset of self-gravitation is approximately

$$\begin{aligned} M_{\rm sg} &= \frac{4\pi\rho_{\rm c} r_{\rm th}^3}{3} \\ &= 0.9\times 10^{17}\ {\rm g}\left(\frac{m_\chi}{10^{10}\ {\rm GeV}}\right)^{-\frac{3}{2}}T_8^{\frac{3}{2}}\rho_6^{-\frac{1}{2}}. \end{aligned} \tag{27}$$

The timescale for reaching this self-gravitating phase is minimized when the DM capture rate saturates to the geometric limit, as described in Eq. (11). Under this condition, the time required to accumulate the critical number of DM particles is given by

$$\begin{aligned} \frac{M_{\rm sg}/m_\chi}{\dot{C}_{\rm geo}} &\approx 4.2\times 10^{-3}\ {\rm Gyr}\,\rho_6^{-\frac{1}{6}}T_8^{\frac{3}{2}}\left(\frac{M_c}{0.1M_\odot}\right)^{-\frac{4}{3}} \\ &\quad\times\left(\frac{m_\chi}{10^{10}\ {\rm GeV}}\right)^{-\frac{3}{2}}\left(\frac{\rho_\chi}{0.3\ {\rm GeV/cm}^3}\right)^{-1}\left(\frac{\bar{v}}{10^{-3}c}\right). \end{aligned} \tag{28}$$

Hence, for DM masses below 10^8 GeV, the capture rate during the RG phase is insufficient to achieve the collapse condition.

Once the total mass of captured DM particles exceeds the threshold $M_{\rm sg}$, the DM sphere becomes self-gravitating and dynamically unstable, which initiates gravitational collapses. The characteristic free-fall timescale is given by

$$t_{\rm ff} = \sqrt{\frac{1}{4\pi G\rho}} = 1.09\ \ {\rm sec}\,\rho_6^{-\frac{1}{2}}. \tag{29}$$

This timescale is typically much shorter than any relevant timescale associated with pressure-supporting interactions, which ensures that the DM configuration is indeed gravitationally unstable once the collapse condition is met. However, the collapse does not result in an immediate black hole formation; instead, the DM particles rapidly virialize on a timescale comparable to $t_{\rm ff}$.

During this phase, DM particles gain increasingly high velocities, elevating their kinetic energy above the ambient core temperature. Subsequent collisions with stellar nuclei cause the DM core to dissipate energy and shrink further in size. This contraction continues until the DM velocity approaches $\sim 0.02c$, beyond which the nuclear form factor becomes strongly suppressed, significantly reducing the energy loss efficiency. Beyond this velocity, scattering could potentially disrupt nuclei, but this is beyond the scope of this paper. For analysis, we conservatively terminate the collapse process when the typical DM velocity reaches $v_{\rm cut} = 0.02c$ and do not consider black hole formation (and following heating via evaporation). The physical consequences of such a collapse, particularly in terms of energy deposition and heating of the surrounding stellar material, will be explored in the next section.

E. Numerics

By means of the full network stellar evolution code, we perform numerical analyses based on low-mass stellar models with initial stellar parameters (mass and composition) relevant to RGB stars in galactic globular clusters. A detailed description of the code and its setup is reported in Ref. [36]. In particular, we adopt an initial stellar mass of $0.83M_\odot$, metallicity of $Z = 0.001$, and initial helium abundance $Y = 0.25$. The initially homogeneous stellar structure then evolves through the pre-main sequence, main sequence, and RGB phases, up to the helium flash at the TRGB, where the model age is 12.2 Gyr, close to the average globular cluster age (11–13 Gyr).

Conventionally, the helium flash is assumed to begin when the luminosity generated by the activation of the triple-α nuclear reactions is 10^2 times the stellar luminosity. For the adopted model, this corresponds to a TRGB bolometric magnitude of $M_{\rm bol} = 4.75 - 2.5\log L/L_\odot = -3.64$ that aligns with the measured values for a globular cluster with a low metallicity of about $Z = 0.001$. For instance, the well-studied globular cluster NGC 5904 (M5) in the northern hemisphere, which has nearly the same metallicity as our stellar models, exhibits a TRGB bolometric magnitude of $M_{\rm bol} = -3.63 \pm 0.26$ (see Table 6 of Ref. [36]). The consistency between theory and observation implies that any nonstandard physics can be accommodated only if its effect on the TRGB luminosity remains within observational uncertainties.

Accordingly, if DM capture process (including ingress, thermalization, and self-gravitating collapse) takes place within the RGB timescale as described in previous subsections, we assess whether the helium flash is triggered earlier, at a time $t_{\rm end}$, when the stellar luminosity falls short of the standard TRGB value by $\log_{10}[|\Delta L|/L_\odot] = 0.13$, corresponding to a bolometric magnitude offset of $\Delta M_{\rm bol} = 0.325$. This threshold closely matches the conservative 95% confidence level adopted in Ref. [36], ensuring that our predictions remain consistent with observations. We further assume that the stellar structure is unaffected by DM capture prior to $t_{\rm end}$, so the only modification is an earlier helium flash induced by heating from the DM core collapse.

Figure 2 illustrates the key profile parameters of the core radius $R_{\rm c}$ (black), the core mass $M_{\rm c}$ (red), the core temperature T_c (blue), and the core density ρ_c (green) from 1 Gyr up to $t_{\rm end}$. As discussed above, we define the core boundary in terms of the escape velocity profile, taking $R_{\rm c}$ to be the radius at which $v_{\rm esc}(R_{\rm c}) = \sqrt{2/3}v_{\rm esc}(0)$. This definition captures the approximately homogeneous central region, where the density profile is nearly flat. The resulting homogeneity supports the straight-line approximation for incoming DM trajectories within the region that dominates the scattering probability. This restriction is conservative, as it neglects potential scattering sites at larger radii and because realistic trajectories are generally more centrally focused than straight lines. Moreover, we verify that the optical depth controlling DM interactions and capture is dominated by this core region, so that our semianalytic estimates remain consistent in the context of the full stellar model.

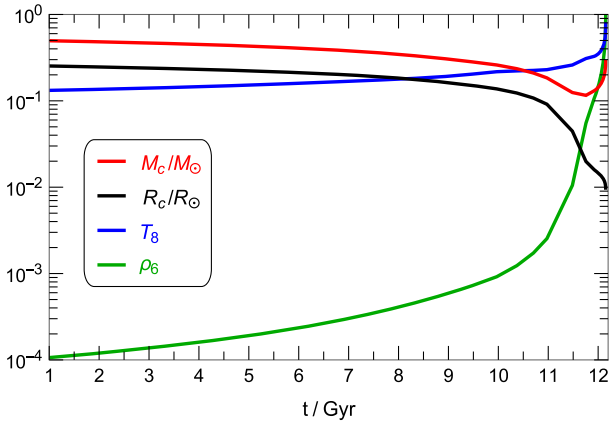


FIG. 2. Evolution of the core mass (red), core radius (black), central temperature (blue), and central density (green). See the text for our operational definition of the core, based on the escape-velocity criterion relevant for DM capture.

In Fig. 3, we show the total number of captured DM particles (blue curve) as a function of time, for a benchmark mass of $m_\chi = 10^{12}$ GeV and a DM-nucleon cross section of $\sigma_{\chi N} = 3 \times 10^{-38}$ cm^2. A sizable number of DM particles are captured during the RG phase, despite its relatively short duration of approximately 1 Gyr. This behavior is consistent with the scaling in Eq. (10). In the weak interaction regime, where the capture rate scales linearly with the elastic scattering cross section, we find $\dot{\mathcal{C}} \propto M_c^3/R_c^2$. Using characteristic core parameters for the main sequence ($M_c \simeq 0.5M_\odot$, $R_c \simeq 0.2R_\odot$) and for the RG phase ($M_c \simeq 0.2M_\odot$, $R_c \simeq 0.01R_\odot$) as shown in Fig. 2,

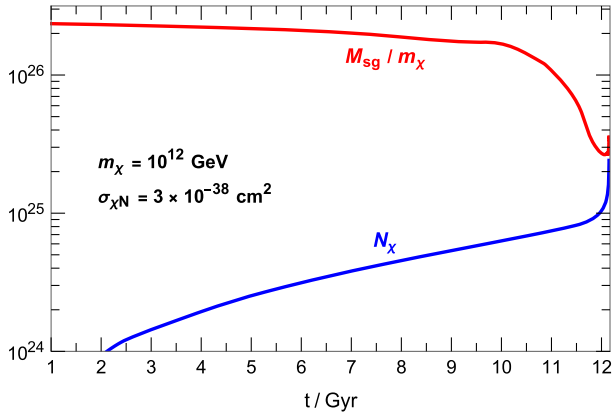


FIG. 3. Evolution of the total number of accumulated DM particles N_χ (blue) and the threshold number for self-gravitation $M_{\rm sg}/m_\chi$ (red), with the DM mass of $m_\chi = 10^{12}$ GeV and the DM-nucleon cross section of $\sigma_{\chi N} = 3 \times 10^{-38}$ cm^2.

the capture efficiency during the RG phase is enhanced by a factor of roughly 30 compared to the main sequence. This enhancement compensates for the shorter duration, which results in a total number of captured particles during the RG phase that is comparable to the main sequence contribution. For comparison, we also plot the evolution of the critical number of DM particles required for the onset of self-gravitation ($N_{\rm sg}$, red), which signals the transition to a gravitationally unstable DM core and potential collapse. This comparison provides a useful check on whether the captured DM population can trigger sufficient localized heating to ignite helium burning. As the plot indicates, the sharply increased capture rate during the RG phase makes the final snapshot particularly relevant for determining whether the captured DM population reaches the collapse threshold, as we will examine in detail in the next section.

III. DARK MATTER-INDUCED HELIUM IGNITION IN RED GIANTS

We now turn to the potential consequences of DM collapse, most notably the premature ignition of helium in the RG core, and discuss possible observational implications. If the heating induced by the collapsing DM core is efficient enough, it can raise the temperature of a portion of the surrounding stellar material to the point where the nuclear reaction rate for helium burning, specifically the triple-α process, becomes large enough to sustain itself. This can trigger a thermal runaway, ultimately igniting the entire helium core before the standard temperature and pressure conditions for helium flash are met.

Although the helium flash itself is not directly observable since most of the released energy is absorbed in lifting the electron degeneracy of the core, its premature onset can leave observable imprints. One such consequence is a decrease in the luminosity at the TRGB. In standard stellar evolution, initially low-mass stars (with $M \lesssim 2M_\odot$) undergo helium ignition when the core reaches a temperature of $T_{\rm c} \sim 10^8$ K and a density of $\rho_{\rm c} \sim 10^6$ g/cm^3. However, if the helium flash is triggered earlier (e.g., at a lower core mass due to DM-induced heating), the correlated tip luminosity of RG would be reduced. Such variations can provide a novel avenue to constrain DM properties. Moreover, since the TRGB has been proposed as a type of standard candle, premature helium ignition may have implications for the reliability of this distance indicator.

The condition for helium ignition is determined by the balance between nuclear heating and conductive or radiative cooling within a localized region of the core. This leads to the concept of a "trigger mass" $M_{\rm tr}$, defined as the minimal mass of core material that must reach a critical temperature for thermal runaway to occur. As for the contribution from plasmon neutrino cooling [58], we have confirmed that it is important only around TRGB, while it is subdominant when DM heats up the core material above 10^8 K. Therefore, we can safely neglect this effect in our discussion. In the following, we examine whether a collapsing DM core can deposit sufficient energy (through elastic scatterings or annihilation) to heat a region of mass $M_{\rm tr}$ above the ignition threshold.

A. Trigger mass for helium ignition

We begin by considering a localized, overheated region that forms within the helium core. The excess heat from this region begins to diffuse outward via conduction or radiative diffusion, effectively cooling the region. Simultaneously, the elevated temperature enhances helium burning through the triple-α process, which generates nuclear energy and may further raise the temperature. Whether the thermal disturbance dissipates or triggers helium ignition depends on the competition between heat loss and nuclear energy generation [43].

This competition is characterized by two timescales: the diffusion timescale $t_{\rm diff}$ and the nuclear burning timescale $t_{\rm burn}$. If $t_{\rm diff} \gg t_{\rm burn}$, nuclear energy accumulates faster than it is lost, which results in a thermonuclear runaway that ignites the entire helium core. Conversely, if $t_{\rm diff} \lesssim t_{\rm burn}$, the excess heat is efficiently conducted away before runaway conditions are achieved.

For a heated region of characteristic size δ with temperature T_b, the diffusion timescale is approximated as

$$t_{\rm diff} \sim \frac{\delta^2}{D}, \tag{30}$$

where D is the thermal diffusivity of the medium. The nuclear burning timescale reads

$$t_{\rm burn} \sim \frac{\epsilon_{\rm th}}{\dot{S}}, \tag{31}$$

where $\epsilon_{\rm th}$ denotes the excess thermal energy per unit mass, and $\dot{S}$ is the local nuclear energy generation rate. Equating these two timescales, $t_{\rm diff} \sim t_{\rm burn}$, yields the minimum size of δ necessary for runaway helium ignition. This defines the trigger mass [43,44],

$$M_{\rm tr} = \frac{4\pi}{3}\delta^3\rho_{\rm c} \sim \frac{4\pi}{3}\left(\frac{\lambda_{\rm eff} v_c \epsilon_{\rm th}}{\dot{S}}\right)^{\frac{3}{2}}\rho_{\rm c}, \tag{32}$$

where we use $D \sim \lambda_{\rm eff} v_c$, with the effective mean free path $\lambda_{\rm eff}$ and the thermal velocity of the conducting particles v_c. The total energy input required to heat this region is roughly given by $M_{\rm tr}\epsilon_{\rm th}$. This order-of-magnitude estimate follows the treatment in Ref. [43], and agrees well with more detailed numerical results.

The excess thermal energy per unit mass can be expressed as

$$\epsilon_{\rm th} = \int_{T_c}^{T_b} c_m dT, \tag{33}$$

where c_m is the specific heat per unit mass, defined as $c_m \equiv (\partial\epsilon_{\rm f}/\partial T)/\rho_{\rm c}$, with the thermal free energy density $\epsilon_{\rm f}$. For a nonrelativistic, fully ionized medium, the heat capacity is controlled by contributions from electrons and helium nuclei. In the helium-rich medium, we exploit the following analytic approximations:

$$[c_m]_{e^-} = \begin{cases} \frac{m_e p_{\rm F} T}{3\rho_{\rm c}} & \text{for } T < T_{\rm deg} \\ \frac{3}{m_{\rm He}} & \text{for } T \geq T_{\rm deg} \end{cases}, \tag{34}$$

$$[c_m]_{\rm He} = \frac{3}{2m_{\rm He}}, \tag{35}$$

where $p_F = (3\pi^2 n_e)^{1/3}$ is the electron Fermi momentum, and $T_{\rm deg} = (p_F^2/2m_e)(3/\pi^2)$. These approximations are valid for temperatures below 10^9 K, beyond which electrons become relativistic and a contribution from photons is non-negligible. In this work, we focus on the nonrelativistic regime.

Next, we estimate the effective heat conductivity in the RG helium core, which determines how DM-induced heating competes with conductive cooling. Since thermal conduction receives contributions from both radiative (via photon) and conductive (via electron) diffusions [59–61], the effective mean free path for conducting particles in the material reads

$$\lambda_{\rm eff} = \lambda_e + \lambda_r, \tag{36}$$

where λ_e and λ_r are the mean free paths for electron and photon diffusion, respectively. A larger $\lambda_{\rm eff}$ implies more efficient conduction, as energy is transported over longer distances. We provide the detailed derivation of the mean free paths in Appendix B.

The energy generation rate from the triple-α process reads [62]

$$\dot{S} = \frac{Q_{3\alpha} r_{3\alpha}}{\rho_{\rm core}} \simeq 3.2 \times 10^{26} \frac{\rm GeV}{\rm s \cdot g} \rho_6^2 T_{b8}^{-3} \exp\left[-\frac{44}{T_{b8}}\right], \tag{37}$$

where $Q_{3\alpha} = 3m_{^4\rm He} - m_{^{12}\rm C} = 7.275$ MeV is the net energy release per reaction, $r_{3\alpha}$ is the resonant reaction rate of the triple-α process, and we define $T_{b8} \equiv T_b/10^8$ K.

Substituting the above expressions for $\epsilon_{\rm th}$, $\dot{S}$, and $\lambda_{\rm eff}$ into Eq. (32), we obtain the trigger mass required to initiate helium ignition. Figure 4 shows $M_{\rm tr}$ as a function of the burning temperature T_b, assuming the core temperature $T_8 = 1$ and density $\rho_6 = 1$. We confirm that our results are in good order-of-magnitude agreement with previous estimations of the trigger mass in Ref. [44]. We also demonstrate the time evolution of the trigger mass, based on our stellar evolution simulation with the benchmark burning temperature of $T_{b8} = 6$, the result of which is shown in Fig. 5.

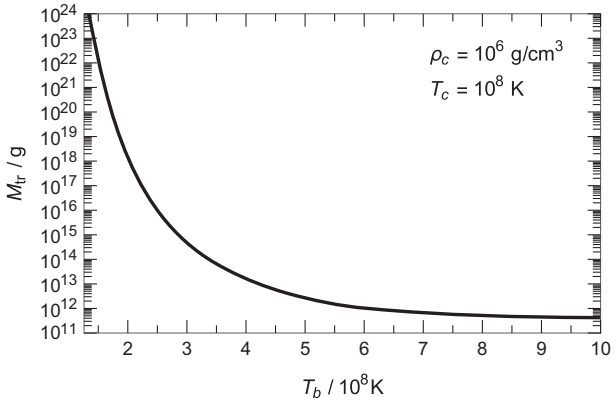


FIG. 4. Trigger mass for the helium ignition, $M_{\rm tr}$, as a function of burning temperature T_b, with $\rho_c = 10^6$ g/cm^3 and $T_c = 10^8$ K as the typical conditions of the RG core.

In summary, if DM-induced heating raises the temperature within a region of mass greater than $M_{\rm tr}$, such that the point lies above the corresponding curve in Fig. 5 at a respective time, the released nuclear energy from helium burning can sustain the temperature and ignite the surrounding material. This localized ignition then initiates a thermal runaway that propagates through the helium core, eventually triggering the helium flash.

B. DM heating and diffusion

Once DM particles in an RG form a self-gravitating core, they undergo gravitational free fall and gradually lose

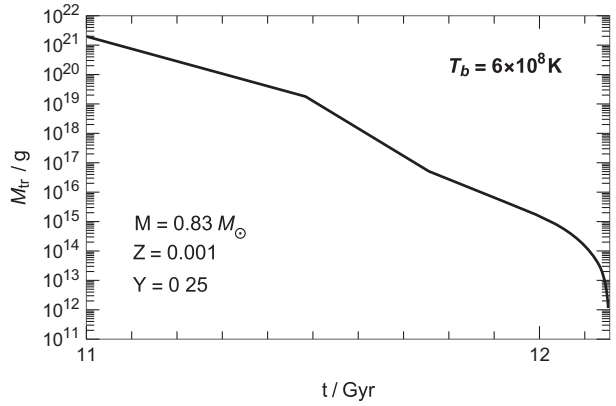


FIG. 5. Evolution of the trigger mass for the helium ignition, $M_{\rm tr}$, based on the stellar evolution simulation.

energy through interactions with ambient helium nuclei. This leads to a contraction of the DM core. There are two key processes contributing to this contraction: elastic scatterings with nuclei, as discussed earlier, and DM self-annihilation, which becomes increasingly important as the DM number density rises during collapse.

For efficient heating of the stellar medium, we require that annihilation becomes significant only after the DM core collapses to sufficiently high densities. If annihilation occurs too early, it can deplete the DM population before the core reaches the conditions necessary for efficient energy deposition. A conservative criterion is that the DM annihilation timescale prior to collapse exceeds the typical RG lifetime of $\sim$1 Gyr.

We denote the annihilation cross section by $\sigma_{\rm ann}$. In the context of the unitarity limit for the DM annihilation, we parametrize $\sigma_{\rm ann} v_\chi$ in terms of the DM mass as

$$\sigma_{\rm ann} v_\chi \equiv \frac{\alpha_\chi^2}{m_\chi^2}, \tag{38}$$

where α_χ accounts for an effective coupling between DM and SM particles. Here, we assume that the s-wave contribution is not suppressed, so that $\sigma_{\rm ann} v_\chi$ remains constant.

The annihilation timescale at the onset of collapse, where DMs are thermalized as described above, is given by

$$[t_{\rm ann}]_{\rm col} = \frac{1}{n_\chi^{\rm th} \sigma_{\rm ann} v_\chi}, \tag{39}$$

where the thermalized DM number density is

$$n_\chi^{\rm th} = \frac{M_{\rm sg}/m_\chi}{(4\pi/3) r_{\rm th}^3} = \frac{\rho_c}{m_\chi}. \tag{40}$$

Requiring $t_{\rm ann} \gtrsim 1$ Gyr yields a lower bound on the DM mass to ensure late-onset annihilation, as follows:

$$m_\chi \gtrsim 1.3 \times 10^9 \ {\rm GeV} \rho_6^{\frac{1}{3}} \left(\frac{\alpha_\chi}{0.1}\right)^{\frac{2}{3}}. \tag{41}$$

This implies that, in contrast to the WIMP DM case, the annihilation of DM with $m_\chi \gtrsim 10^9$ GeV typically remains inefficient even as its density grows large enough to induce gravitational collapse.

After collapse, the evolution of the DM core is governed by the total energy change of DM particles, combining contributions from scattering and annihilation, as follows:

$$\frac{dE_\chi}{dt} = \left.\frac{dE}{dt}\right|_{\rm scat} + \left.\frac{dE}{dt}\right|_{\rm ann}. \tag{42}$$

For a homogeneous DM distribution within the core, the virial theorem relates the average kinetic and potential energies of a DM particle,

$$2\langle K_\chi \rangle = -\langle V_\chi \rangle, \tag{43}$$

with

$$\langle K_\chi \rangle = \frac{1}{2} m_\chi \bar{v}_\chi^2, \qquad \langle V_\chi \rangle = -\frac{3}{5}\frac{G N_\chi m_\chi^2}{r_\chi}, \tag{44}$$

where $\bar{v}_\chi$ is the average DM velocity, and r_χ is the characteristic size of the DM core. The total DM energy is then

$$E_\chi = N_\chi(\langle K_\chi \rangle + \langle V_\chi \rangle) \simeq \frac{1}{2} N_\chi \langle V_\chi \rangle, \tag{45}$$

where N_χ is the total number of DM particles.

The energy loss rate due to elastic scatterings between DM and nuclei is estimated as

$$\begin{aligned} \left.\frac{dE}{dt}\right|_{\rm scat} &\simeq -N_\chi \langle K_\chi \rangle \frac{\beta}{2} t_{\rm scat}^{-1} \\ &\simeq \frac{1}{2} E_\chi \beta (n_{\rm He} \sigma_{\chi{\rm He}} v_{\rm rel}). \end{aligned} \tag{46}$$

The second term on the rhs of Eq. (42) accounts for the total DM energy change through the DM pair annihilation. Considering that each annihilation event removes two (identical) particles and releases their combined energy, we find

$$\begin{aligned} \left.\frac{dE}{dt}\right|_{\rm ann} &\simeq \frac{dN_\chi}{dt}(\langle K_\chi \rangle + 2\langle V_\chi \rangle) \\ &\simeq -3 E_\chi (n_\chi \sigma_{\rm ann} v_\chi), \end{aligned} \tag{47}$$

where in the second line, we use the relation of

$$\frac{1}{N_\chi}\frac{dN_\chi}{dt} = -n_\chi \sigma_{\rm ann} v_\chi. \tag{48}$$

In the absence of annihilation, the total number of DM particles is conserved, and the total DM heating rate is governed solely by elastic scatterings. This heating rate is maximized when the DM velocity reaches the decoherence threshold, $v_{\rm cut} \approx 0.02c$, as described in Sec. II D. The maximum elastic heating rate is given by

$$\begin{aligned} \dot{Q}_{\rm scat} &= -\left[\left.\frac{dE}{dt}\right|_{\rm scat}\right]_{\bar{v}_\chi = v_{\rm cut}} \\ &\simeq \frac{1}{4} M_{\rm sg} v_{\rm cut}^2 \beta (n_{\rm He} \sigma_{\chi{\rm He}} v_{\rm cut}), \end{aligned} \tag{49}$$

where the prefactor indicates the mean DM energy loss per DM-He collision, and the term in the parentheses corresponds to the DM-He elastic scattering rate. The corresponding DM number density at this point reads

$$[n_\chi]_{\rm cut} = n_\chi^{\rm th}\left(\frac{m_\chi v_{\rm cut}^2}{3T_c}\right)^3. \tag{50}$$

The total contraction timescale is approximately given by $2/(n_{\rm He}\sigma_{\chi{\rm He}}v_{\rm cut})$, which is comparable to the thermalization timescale $t_{\rm th}$ in Eq. (25).

In a more realistic scenario, DM self-annihilation becomes significant as the density increases due to gravitational contraction. Taking the derivative of Eq. (45), we have

$$\frac{1}{E_\chi}\frac{dE_\chi}{dt} = \frac{1}{2N_\chi}\frac{dN_\chi}{dt}\langle V_\chi\rangle + \frac{1}{2}N_\chi\left(\frac{\partial\langle V_\chi\rangle}{\partial N_\chi}\frac{dN_\chi}{dt} + \frac{\partial\langle V_\chi\rangle}{\partial r_\chi}\frac{dr_\chi}{dt}\right), \tag{51}$$

which allows us to determine the evolution of r_χ. Equating dE_χ/dt to the sum of Eqs. (46) and (47), we arrive at

$$-\frac{1}{r_\chi}\frac{dr_\chi}{dt} = \frac{\beta}{2}(n_c\sigma_{\chi{\rm He}}v_{\rm rel}) - n_\chi\sigma_{\rm ann}v_\chi. \tag{52}$$

This yields the evolution equation for the DM number density:

$$\begin{aligned}\frac{1}{n_\chi}\frac{dn_\chi}{dt} &= \frac{1}{N_\chi}\frac{dN_\chi}{dt} - \frac{3}{r_\chi}\frac{dr_\chi}{dt}\\ &\simeq \frac{3}{2}\beta n_c\sigma_{\chi{\rm He}}v_{\rm rel} - 4n_\chi\sigma_{\rm ann}v_\chi.\end{aligned} \tag{53}$$

As a result, the DM number density increases until it reaches a saturation point (i.e., $dn_\chi/dt = 0$), where the contraction due to elastic scattering is balanced by annihilation-induced depletion, as follows:

$$[n_\chi]_{\rm sat} = \frac{3\beta n_c\sigma_{\chi{\rm He}}v_{\rm rel}}{8\sigma_{\rm ann}v_\chi}. \tag{54}$$

This saturation can occur if $[n_\chi]_{\rm cut} > [n_\chi]_{\rm sat}$, which is generally satisfied more easily than the constraint in Eq. (41) to prohibit precollapse annihilation. Specifically, this condition gives

$$m_\chi \gtrsim 3\times10^{-14}\ {\rm GeV}\left(\frac{\sigma_{\chi{\rm He}}}{10^{-37}\ {\rm cm}^2}\right)\left(\frac{v_{\rm rel}}{v_{\rm th}}\right)\left(\frac{\alpha_\chi}{0.1}\right)^2, \tag{55}$$

where we have assumed the thermal velocity of helium nuclei dominates the relative velocity as a conservative estimation. Clearly, this condition is much easier to satisfy than Eq. (41), so the saturation point is always reached in the parameter space of our interest if we turn on the annihilation. Since annihilation becomes significant near the saturation point, where the total DM number N_χ begins to diminish exponentially, the maximal DM heating rate from annihilation, releasing the DM rest mass energy, is approximately given by

$$\begin{aligned}\dot{Q}_{\rm ann} &\simeq m_\chi N_{\rm sg}[n_\chi]_{\rm sat}\sigma_{\rm ann}v_\chi\\ &= \frac{3}{8}M_{\rm sg}\beta n_c\sigma_{\chi{\rm He}}v_{\rm rel}.\end{aligned} \tag{56}$$

This rate significantly exceeds the maximum elastic heating rate in Eq. (49) (in the absence of DM self-annihilation). The ratio between them can be found as

$$\frac{\dot{Q}_{\rm ann}}{\dot{Q}_{\rm scat}} = \frac{3}{2}\frac{v_{\rm rel}}{v_{\rm cut}}\frac{1}{v_{\rm cut}^2} = \mathcal{O}(10^3), \tag{57}$$

where again we have conservatively taken $v_{\rm rel} = v_{\rm th}$. This leads to a significant enhancement of the heating efficiency and, therefore, a much stronger constraint from the annihilation of DM particles than that with only elastic scatterings.

The localized overheating caused by energy deposition from collapsed DM particles can be redistributed via thermal diffusion into the surrounding cooler regions. As DM heating continues, this process gradually raises the temperature of nearby material until the heating and diffusion rates are balanced. For a diffusion region of size r, the diffusion rate reads

$$\begin{aligned}\dot{Q}_{\rm diff} &= -\frac{16\pi r^2 c}{3\kappa\rho_c}aT_c^3\frac{dT}{dr}\\ &\simeq -\frac{16\pi^3 r}{45}\lambda_{\rm eff}T_c^3(T_b - T_c),\end{aligned} \tag{58}$$

where $a = 4\sigma/c$ is the radiation constant with the Stefan-Boltzmann constant σ, and κ denotes the opacity of the conducting medium with the relation of $(\kappa\rho_c)^{-1} \simeq \lambda_{\rm eff}$.

If the heating rate $\dot{Q}_\chi$ exceeds the diffusion rate $|\dot{Q}_{\rm diff}|$, helium material within radius r can be heated above T_b. As discussed in Sec. III A, if the heated region exceeds the volume of the corresponding trigger mass required for helium ignition at temperature T_b, this imbalance results in a runaway burning process, ultimately igniting the entire stellar core.

To quantify this condition, we adopt a benchmark burning temperature of $T_b = 6\times10^8$ K, for which the critical mass condition is nearly saturated as shown in Fig. 4; see Fig. 5 for the trigger mass at a respective time. The corresponding trigger radius $r_{\rm tr} \simeq 62$ cm is significantly larger than the typical size of the collapsed DM core around $r_{\rm cut} \simeq 1.7\times10^{-8}$ cm. Therefore, our diffusion-based ignition criterion is self-consistent: the DM heating

can be considered pointlike relative to the ignition region of interest. The diffusion rate at this threshold scale determines the critical DM heating rate for successful helium ignition. Imposing that DM heating does not exceed this critical diffusion rate, i.e., $\dot{Q}_\chi < |\dot{Q}_{\rm diff}|_{r=r_{\rm tr}}$, places an upper bound on the DM-nucleus interaction cross section.

C. Results

In Fig. 6, the red lines indicate the DM parameter space, where the DM heating rate can exceed the diffusion rate that allows for runaway helium ignition in the stellar core. The pale red line ($\dot{Q}_{\rm sca} = |\dot{Q}_{\rm diff}|$) corresponds to the case without DM annihilation, where heating arises solely from DM-nucleus elastic scattering (i.e., kinetic heating), as given by Eq. (49). The solid red line ($\dot{Q}_{\rm ann} = |\dot{Q}_{\rm diff}|$) includes the additional contribution from DM self-annihilation, described by Eq. (56), which enhances the heating rate by roughly three orders of magnitude as discussed above.

However, the red contours indicating successful DM-induced heating are only valid if all prerequisite conditions for DM ingress, thermalization, and collapse (outlined in Sec. II) are satisfied. The conditions for ingress and thermalization can be formulated in terms of characteristic timescales, each of which must be shorter than the RG lifetime, approximately $t_{\rm RG} \approx 1$ Gyr:

(i) $t_{\rm ingress} < t_{\rm RG}$: after being captured, DM particles gradually lose energy through repeated scatterings with nuclei. Ingress is complete when their orbits become fully confined within the RG core. This must occur early enough to enable subsequent evolution.

(ii) $t_{\rm th} < t_{\rm RG}$: once confined, DM particles continue to scatter until their kinetic energy becomes comparable to the core temperature. The thermalization process must be completed within the RG lifetime.

The other condition for DM collapse reads:

(i) $N_\chi(t_{\rm end}) > M_{\rm sg}/m_\chi$: after thermalization, the DM distribution remains extended until its density exceeds that of the ambient stellar medium. At this point, DM self-gravity dominates, and the DM core collapses. For this to contribute to helium ignition, the collapse must occur within the stellar lifetime.

Here, as discussed in Sec. II E, $t_{\rm end}$ denotes the truncated evolution time, which is chosen to ensure that a premature helium flash results in a luminosity sufficiently lower than the TRGB value, accounting for theoretical and observational uncertainties. We note that for cross sections larger than this threshold, DM collapse can occur earlier than $t_{\rm end}$, but the corresponding heating-cooling competition condition is typically satisfied without difficulty. Furthermore, due to the significantly enhanced capture efficiency during the RG phase, additional DM captured and accumulated later in the evolution can also readily fulfil this collapse condition.

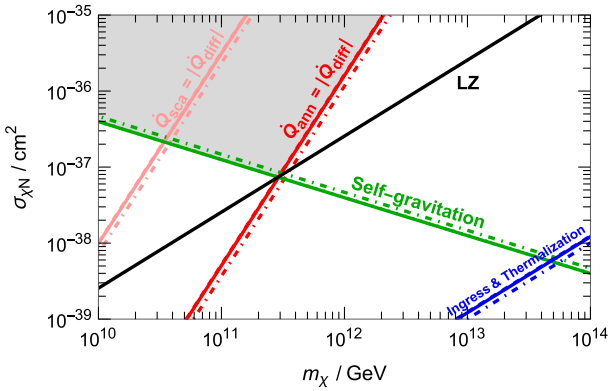


FIG. 6. Constraints on the spin-independent DM-nucleon cross section. The red (annihilation heating) and pale red (elastic-scattering heating only) lines show the ignition boundaries, defined by our runaway condition in the heated region. The blue line marks the combined requirement that captured DM can ingress to the core and thermalize within the relevant stellar timescale. The green line indicates the threshold above which the captured DM becomes self-gravitating. The gray-shaded region is excluded: it corresponds to parameter points that simultaneously satisfy the capture and transport requirements (capture + ingress + thermalization), reach self-gravitation, and exceed the corresponding ignition boundary (pale red), implying a DM-induced premature helium flash under our adopted stellar profile and localized-heating treatment. Solid lines correspond to the benchmark model with $(M, Z) = (0.83M_\odot, 0.001)$. For comparison, the region above the black line is excluded by terrestrial direct detection experiments [10]. To confirm the robustness of our results, we also show results obtained using alternative stellar-evolution profiles: $(0.83M_\odot, 0.0001)$ (dot-dashed lines) and $(0.9M_\odot, 0.001)$ (dashed lines).

In Fig. 6, the blue and green lines represent the boundaries imposed by the combined ingress and thermalization conditions, and the self-gravitation criterion, respectively. The region above all these lines defines the DM parameter space in which capture, collapse, and subsequent heating can occur within the relevant RG evolutionary timescale, enabling the subsequent heating required for helium ignition.

As shown in Fig. 6, the ingress and thermalization conditions (blue line) are easily satisfied across a broad range of DM parameters and thus impose only mild constraints. The self-gravitation condition yields a more stringent bound, with the green line representing the critical line above which DM particles can undergo collapse within the RG lifetime. In the absence of annihilation, elastic scattering alone can provide sufficient heating to ignite helium, but the corresponding parameter region (pale red line) lies above the exclusion limit from current direct detection experiments. However, when DM self-annihilation is involved, the heating rate is significantly enhanced, shifting the viable region downward in the parameter space (red line). This accounts for a significant

sensitivity of RGs in parameter space for HDM, in particular with masses around 10^{11} GeV and spin-independent nucleon cross sections on the order of 10^{-37} cm^2 (gray-shaded region). This result highlights a novel astrophysical sensitivity to HDM candidates comparable to the reach of existing terrestrial searches.

As a remark, to evaluate the sensitivity of our results to the underlying stellar model, we repeat the full analysis using additional RG profiles with different initial masses and metallicities, chosen to remain consistent with the ages and metallicities of the halo globular clusters relevant for TRGB-based constraints. In particular, besides our benchmark model $(M, Z) = (0.83M_\odot, 0.001)$ illustrated by solid lines, which serves as a representative case, we take into account $(0.83M_\odot, 0.0001)$ to probe lower metallicity (dot-dashed line) and $(0.9M_\odot, 0.001)$ to probe a modest increase in mass corresponding to an younger ($\sim$11 Gyr) population (dashed line). We realize that the resulting exclusion contours are nearly unchanged and largely overlap those of the benchmark case, which indicates that our results are robust against realistic variations in mass and metallicity within the parameter range relevant to halo globular clusters. In practice, the residual uncertainty associated with these stellar-profile variations is small compared with other theoretical uncertainties, most notably those related to the DM capture and subsequent collapse/heating phenomenology.

IV. CONCLUSION AND DISCUSSION

In this work, we have investigated the possibility that captured DM inside RG cores can trigger premature helium ignition via localized heating. Such an event would alter the stellar evolutionary path of low-mass stars and their observational consequences, particularly lowering the luminosity at the TRGB. This provides a novel astrophysical probe of DM interactions with baryonic matter.

We began by analyzing DM capture via elastic scattering with nuclei in the RG core and identified the parametric regimes where the capture rate scales linearly with the scattering cross section and where it saturates at the geometric limit. We derived analytic expressions for the capture rate that agree with the full numerical results across a broad range of DM masses and cross sections (Sec. II A). Once captured, the DM particles accumulate in the stellar core. For most of the relevant parameter space, DM ingress (Sec. II B) and thermalization (Sec. II C) occur on relatively short timescales, and the DM population becomes concentrated in a compact region. When the total DM mass exceeds the self-gravitating threshold $M_{\rm sg}$, the DM core becomes unstable and collapses under its own gravity (Sec. II D). This collapse proceeds through a sequence of virialized configurations regulated by scatterings with the stellar medium.

This dense, compact DM core can serve as a localized heat source, either via annihilation or continued elastic scattering, which potentially raises the temperature of the surrounding material. We estimated the critical trigger mass and radius for helium ignition by balancing the nuclear energy release against conductive diffusion losses (Sec. III A). Using this framework, we developed a self-consistent diffusion-based ignition criterion to compare the DM heating rate to the diffusive losses over the relevant spatial scale (Sec. III B).

The resulting constraints on DM parameter space are summarized in Fig. 6. Ingress and thermalization conditions (blue line) impose only mild restrictions, while the self-gravitating collapse sets a stronger bound (green line). In the absence of annihilation, elastic scattering can still provide sufficient heating (red line), though this region is already excluded by current direct detection bounds. However, when annihilation is included, the heating rate is significantly enhanced by a factor of $1/v_{\rm cut}^2 \sim 10^3$ that leads to a sensitive probe of DM as comparable to direct detection searches, particularly for masses around 10^{11} GeV and spin-independent cross sections around 10^{-37} cm^2. We note that the current best direct detection constraint [10] in Fig. 6 is extrapolated from the constraint for the sub-TeV DM and may be less robust in the high-mass, large cross section regime due to potential Earth-shielding effects. Hence, RG observations offer a complementary probe of DM in this otherwise inaccessible regime.

It is noteworthy to compare our results with earlier studies [37–39] that also explore DM-triggered helium flashes in RGs. References [37,39] focus on weak scale DM, $m_\chi \sim 1$ TeV, for which annihilation can become important even before gravitational collapse. In that regime, energy deposition from DM self-annihilation, which is equilibrated with the capture rate, occurs over spatial scales much larger than the thermal radius scale, which implies a heated region that is far more extended than the compact, near pointlike heating relevant to our setup. Consequently, analyses in this mass range generally require a broader hydrodynamical treatment of the stellar response. Reference [38] examines macroscopic DM with masses of 10^{17}–10^{20} g, which also leads to heating over large spatial scales comparable to a nongravitational interaction size. While all these studies, including ours, apply similar diffusion-based runaway criteria, our analysis is distinct in exploring helium ignition under much smaller ignition radii, relevant for DM in the mass regime, where precollapse annihilation is negligible. This allows for a significant localized heating scenario and a correspondingly more stringent ignition condition.

In conclusion, RGB stars provide a sensitive and complementary probe of heavy DM with sizable interactions. Our findings highlight a novel astrophysical window into DM that could be further explored with improved stellar modeling and future observational advances.

ACKNOWLEDGMENTS

We thank Andrea Caputo, Hyungjin Kim, Jorge Martin-Camalich, and Meng-Ru Wu for useful discussions. S. G., M. H., C. S. S., and S. Y. are supported by IBS under Project Code No. IBS-R018-D1. C. S. S. is supported by Global-Learning & Academic research institution for Master's PhD students, and Postdocs (G-LAMP) Program of the National Research Foundation of Korea (NRF) grant funded by the Ministry of Education (No. RS-2025-25442707), and by the NRF grant funded by the Korean government (MSIT) (No. RS-2026-25498521). O. S. acknowledges the support of the large-program BRAVOSUN funded by the Italian National Institute of Astrophysics.

DATA AVAILABILITY

The data that support the findings of this article are openly available [10,36,43,44].

APPENDIX A: APPROXIMATED DERIVATION OF g_N

In this appendix, we show that the capture probability g_N can be evaluated analytically under a linear approximation, which is valid for $\beta N \ll 1$. Here, β denotes the parameter for the fractional energy loss per DM-nucleus scattering, defined in Eq. (3), and N is the number of scatterings.

From the definition in Eq. (5), we can expand the product inside the step function to first order in β as

$$\prod_{i=1}^{N}(1-\beta x_i) \simeq 1-\beta\sum_{i=1}^{N} x_i. \tag{A1}$$

The capture probability then approximates to

$$g_N \simeq \left[\prod_{i=1}^{N}\int_0^1 dx_i\ f_i(x_i)\right]\Theta\left(-\frac{1}{\beta}\frac{u^2}{\omega^2}+y_N\right), \tag{A2}$$

where we define

$$y_N \equiv \sum_{i=1}^{N} x_i. \tag{A3}$$

Assuming identical and independent distributions for all x_i, such that $f_i(x_i)=f(x_i)$, we can apply the central limit theorem in the large $N\gg 1$ limit. In this case, the distribution of y_N approaches a Gaussian

$$g_N(\omega,\beta) \simeq \int_0^N dy_N\ f_{y_N}(y_N)\Theta\left(-\frac{1}{\beta}\frac{u^2}{\omega^2}+y_N\right), \tag{A4}$$

where f_{y_N} is the probability distribution of y_N, approximated by a Gaussian with mean $N\times \mathrm{E}[x_i]$ and variance $N\times \mathrm{Var}[x_i]$ with $\mathrm{E}[x_i]$ and $\mathrm{Var}[x_i]$ denoting the mean and variance of x_i, respectively.

For a uniform distribution of $x_i\in[0,1]$, i.e., $f(x_i)=1$, we have $\mathrm{E}[x_i]=1/2$ and $\mathrm{Var}[x_i]=1/12$. This results in

$$f_{Y_N}(y_N) \simeq \frac{1}{\sqrt{2\pi}\sqrt{N/12}}\exp\left[-\frac{(y_N-N/2)^2}{N/6}\right]. \tag{A5}$$

The capture probability can be written analytically in terms of the error function (Erf) as

$$g_N \simeq \frac{1}{2}\left(\mathrm{Erf}\left[\sqrt{\frac{3N}{2}}\right]-\mathrm{Erf}\left[\frac{\frac{u^2}{\beta\omega^2}-\frac{N}{2}}{\sqrt{N/6}}\right]\right). \tag{A6}$$

APPENDIX B: MEAN FREE PATHS FOR RADIATIVE AND CONDUCTIVE DIFFUSION IN RED GIANT CORES

In this appendix, we derive the mean free paths of photons and electrons, which are the primary carriers of energy through radiative and conductive diffusion, respectively, in helium-rich cores of RG stars.

Photons in RG cores interact through scattering with free electrons and via inverse bremsstrahlung absorption (free-free absorption). The former is described by Thomson scattering in the nonrelativistic limit, leading to the following opacity [64]:

$$\kappa_{\mathrm{f}\gamma} = \frac{n_e}{\rho_c}\sigma_{\mathrm{Th}} f_\eta \simeq 0.4\left(\frac{Z}{A}\right) f_\eta\ \mathrm{cm^2\ g^{-1}}, \tag{B1}$$

where $A=4$ and $Z=2$ are the atomic and charge numbers of helium nuclei, respectively. The function f_η accounts for suppression due to electron degeneracy [65–69], for which we adopt the analytic fit from Ref. [69].

For inverse bremsstrahlung absorption in the low-temperature regime (where positrons are negligible), the Rosseland mean opacity is given by [70]

$$\kappa_{\mathrm{ff}} = \left[\frac{15}{4\pi^4}\rho_c\int_0^\infty \frac{u^4 e^{-u}du}{(1-e^{-u})^3 n_e\langle\sigma^-\rangle}\right]^{-1}, \tag{B2}$$

where $\langle\sigma^-\rangle$ the thermally averaged cross section for inverse bremsstrahlung. The following relation connects this cross section to temperature and density, as follows:

$$\frac{n_e\langle\sigma^-\rangle}{\rho_c} = 7.4\times 10^2\ \mathrm{cm^2\ g^{-1}}\rho_6 T_8^{-\frac{7}{2}}\frac{g_{\mathrm{He}}}{u^3}, \tag{B3}$$

where $g_{\mathrm{He}}\sim\mathcal{O}(1)$ is the Gaunt factor [70,71]. This leads to an opacity that obeys the Kramers' law in terms of the density and temperature. The total photon mean free path is then given by

$$\lambda_r = \frac{1}{\rho(\kappa_{f\gamma} + \kappa_{ff})}. \tag{B4}$$

The conductive opacity is expressed as

$$\kappa_e = \frac{16\sigma T^3}{3\rho\xi}, \tag{B5}$$

where ξ is the thermal conductivity. In the degenerate regime, ξ takes the form

$$\xi = \frac{\pi^2 n_e T}{3 m_e \nu_e}, \tag{B6}$$

with ν_e the total electron scattering frequency. This includes contributions from both electron-ion (ei) and electron-electron (ee) scattering.

The frequency for electron-ion (Mott) scattering is [59]

$$\nu_{ei} = \frac{4\pi Z^2 \alpha^2}{p_F^2 v_F} n_i \Lambda_{ei}, \tag{B7}$$

where p_F is the electron Fermi momentum, $v_F = p_F/\sqrt{p_F^2 + m_e^2}$ is the Fermi velocity, and n_i is the ion number density. The Coulomb logarithm Λ_{ei} is given by

$$\Lambda_{ei} = \ln\left[\left(\frac{2\pi Z}{3}\right)^{\frac{1}{3}}\left(1.5 + \frac{3}{\Gamma}\right)^{\frac{1}{2}}\right] - \frac{v_F^2}{2}, \tag{B8}$$

with the Coulomb plasma parameter defined as

$$\Gamma = \frac{Z^2\alpha}{T}\left(\frac{4\pi n_i}{3}\right)^{1/3}. \tag{B9}$$

The electron-electron scattering frequency [60,61] incorporates plasma screening effects and follows the fitted expression [72,73]

$$\nu_{ee} = \frac{6\alpha^{\frac{3}{2}}}{\pi^{\frac{5}{2}}} p_F \sqrt{v_F} y I(v_F, y), \tag{B10}$$

where $y \equiv \sqrt{3}\omega_{pl}/T$, with $\omega_{pl} = \sqrt{4\pi\alpha n_e/(p_F^2 + m_e^2)^{1/2}}$ the plasma frequency, and [72,73]

$$I(v_F, y) = \frac{1}{v_F}\left(\frac{10}{63} - \frac{8/315}{1 + 0.0435y}\right)\ln\left[1 + \frac{128.56}{37.1y + 10.83y^2 + y^3}\right] + v_F^3\left(\frac{2.404}{\mathtt{B}} + \frac{\mathtt{C} - 2.404/\mathtt{B}}{1 + 0.1 v_F y}\right)\ln\left[1 + \frac{\mathtt{B}}{\mathtt{A} v_F y + v_F^2 y^2}\right]$$
$$+ \frac{v_F}{1 + \mathtt{D}}\left(\mathtt{C} + \frac{18.52 v_F^2 \mathtt{D}}{\mathtt{B}}\right)\ln\left[1 + \frac{\mathtt{B}}{\mathtt{A} y + 10.83 v_F^2 y^2 + v_F^{8/3} y^{8/3}}\right], \tag{B11}$$

with $\mathtt{A} = 12.2 + 25.2 v_F^3$, $\mathtt{B} = \mathtt{A}\exp[(0.123636 + 0.016234 v_F^2)/\mathtt{C}]$, $\mathtt{C} = 8/105 + 0.05714 v_F^4$, and $\mathtt{D} = 0.1558 y^{1 - 0.75 v_F}$. Summing both contributions,

$$\nu_e = \nu_{ei} + \nu_{ee}, \tag{B12}$$

we can evaluate κ_e using Eq. (B5), and define the electron mean free path as

$$\lambda_e = \frac{1}{\rho\kappa_e}. \tag{B13}$$

Finally, the effective mean free path governing energy diffusion in the RG core is given by the sum of the radiative and conductive contributions, as follows:

$$\lambda_{\text{eff}} = \lambda_r + \lambda_e. \tag{B14}$$

[1] Planck Collaboration, Planck 2018 results. VI. Cosmological parameters, Astron. Astrophys. **641**, A6 (2020).

[2] Y. Sofue and V. Rubin, Rotation curves of spiral galaxies, Annu. Rev. Astron. Astrophys. **39**, 137 (2001).

[3] D. Harvey, R. Massey, T. Kitching, A. Taylor, and E. Tittley, The non-gravitational interactions of dark matter in colliding galaxy clusters, Science **347**, 1462 (2015).

[4] M. Schumann, Direct detection of WIMP dark matter: Concepts and status, J. Phys. G **46**, 103003 (2019).

[5] B. W. Lee and S. Weinberg, Cosmological lower bound on heavy neutrino masses, Phys. Rev. Lett. **39**, 165 (1977).

[6] G. Bertone and D. Hooper, History of dark matter, Rev. Mod. Phys. **90**, 045002 (2018).

[7] J. Billard *et al.*, Direct detection of dark matter—APPEC committee report, Rep. Prog. Phys. **85**, 056201 (2022).
[8] D. S. Akerib *et al.*, Snowmass2021 cosmic frontier dark matter direct detection to the neutrino fog, in *Snowmass 2021* (2022), arXiv:2203.08084.
[9] XENON Collaboration, First dark matter search results from the XENON1T experiment, Phys. Rev. Lett. **119**, 181301 (2017).
[10] LZ Collaboration, First dark matter search results from the LUX-ZEPLIN (LZ) experiment, Phys. Rev. Lett. **131**, 041002 (2023).
[11] K. Griest and M. Kamionkowski, Unitarity limits on the mass and radius of dark matter particles, Phys. Rev. Lett. **64**, 615 (1990).
[12] A. Berlin, D. Hooper, and G. Krnjaic, Thermal dark matter from a highly decoupled sector, Phys. Rev. D **94**, 095019 (2016).
[13] H. Kim and E. Kuflik, Superheavy thermal dark matter, Phys. Rev. Lett. **123**, 191801 (2019).
[14] A. Berlin, WIMPs with GUTs: Dark matter coannihilation with a lighter species, Phys. Rev. Lett. **119**, 121801 (2017).
[15] E. D. Kramer, E. Kuflik, N. Levi, N. J. Outmezguine, and J. T. Ruderman, Heavy thermal dark matter from a new collision mechanism, Phys. Rev. Lett. **126**, 081802 (2021).
[16] R. Frumkin, E. Kuflik, I. Lavie, and T. Silverwater, Roadmap to thermal dark matter beyond the weakly interacting dark matter unitarity bound, Phys. Rev. Lett. **130**, 171001 (2023).
[17] D. Chway, T. H. Jung, and C. S. Shin, Dark matter filtering-out effect during a first-order phase transition, Phys. Rev. D **101**, 095019 (2020).
[18] M. J. Baker, J. Kopp, and A. J. Long, Filtered dark matter at a first order phase transition, Phys. Rev. Lett. **125**, 151102 (2020).
[19] P. Asadi, E. D. Kramer, E. Kuflik, G. W. Ridgway, T. R. Slatyer, and J. Smirnov, Accidentally asymmetric dark matter, Phys. Rev. Lett. **127**, 211101 (2021).
[20] O. Lennon, J. March-Russell, R. Petrossian-Byrne, and H. Tillim, Black hole genesis of dark matter, J. Cosmol. Astropart. Phys. 04 (2018) 009.
[21] L. Morrison, S. Profumo, and Y. Yu, Melanopogenesis: Dark matter of (almost) any mass and baryonic matter from the evaporation of primordial black holes weighing a ton (or less), J. Cosmol. Astropart. Phys. 05 (2019) 005.
[22] D. Hooper, G. Krnjaic, and S. D. McDermott, Dark radiation and superheavy dark matter from black hole domination, J. High Energy Phys. 08 (2019) 001.
[23] T. C. Gehrman, B. Shams Es Haghi, K. Sinha, and T. Xu, Recycled dark matter, J. Cosmol. Astropart. Phys. 03 (2024) 044.
[24] G. G. Raffelt, Stars as Laboratories for Fundamental Physics: The Astrophysics of Neutrinos, Axions, and Other Weakly Interacting Particles (The University of Chicago Press, Chicago, 1996).
[25] W. H. Press and D. N. Spergel, Capture by the sun of a galactic population of weakly interacting massive particles, Astrophys. J. **296**, 679 (1985).
[26] A. Gould, Resonant enhancements in WIMP capture by the earth, Astrophys. J. **321**, 571 (1987).
[27] R. L. Gilliland, J. Faulkner, W. H. Press, and D. N. Spergel, Solar models with energy transport by weakly interacting particles, Astrophys. J. **306**, 703 (1986).
[28] P. Scott, M. Fairbairn, and J. Edsjo, Dark stars at the Galactic Centre—The main sequence, Mon. Not. R. Astron. Soc. **394**, 82 (2009).
[29] J. Casanellas, I. M. Brandão, and Y. Lebreton, Stellar convective cores as dark matter probes, Phys. Rev. D **91**, 103535 (2015).
[30] J. Lopes and I. Lopes, Asymmetric dark matter imprint on low-mass main-sequence stars in the Milky Way nuclear star cluster, Astrophys. J. **879**, 50 (2019).
[31] T. J. Raen, H. Martínez-Rodríguez, T. J. Hurst, A. R. Zentner, C. Badenes, and R. Tao, The effects of asymmetric dark matter on stellar evolution I: Spin-dependent scattering, Mon. Not. R. Astron. Soc. **503**, 5611 (2021).
[32] J. Casanellas and I. Lopes, Towards the use of asteroseismology to investigate the nature of dark matter, Mon. Not. R. Astron. Soc. **410**, 535 (2011).
[33] J. Casanellas and I. Lopes, First asteroseismic limits on the nature of dark matter, Astrophys. J. Lett. **765**, L21 (2013).
[34] J. Casanellas and I. Lopes, The formation and evolution of Young low-mass stars within halos with high concentration of dark matter particles, Astrophys. J. **705**, 135 (2009).
[35] J. Rato, J. Lopes, and I. Lopes, On asymmetric dark matter constraints from the asteroseismology of a subgiant star, Mon. Not. R. Astron. Soc. **507**, 3434 (2021).
[36] O. Straniero, C. Pallanca, E. Dalessandro, I. Dominguez, F. R. Ferraro, M. Giannotti, A. Mirizzi, and L. Piersanti, The RGB tip of galactic globular clusters and the revision of the axion-electron coupling bound, Astron. Astrophys. **644**, A166 (2020).
[37] J. Lopes and I. Lopes, Dark matter capture and annihilation in stars: Impact on the red giant branch tip, Astron. Astrophys. **651**, A101 (2021).
[38] C. Dessert and Z. Johnson, Red-giant branch stellar cores as macroscopic dark matter detectors, Phys. Rev. D **106**, 103034 (2022).
[39] H. Hong and A. C. Vincent, Dark matter limits from the tip of the red giant branch of globular clusters, Phys. Rev. D **110**, 103011 (2024).
[40] F. Capozzi and G. Raffelt, Axion and neutrino bounds improved with new calibrations of the tip of the red-giant branch using geometric distance determinations, Phys. Rev. D **102**, 083007 (2020).
[41] S.-P. Li and X.-J. Xu, Production rates of dark photons and Z' in the Sun and stellar cooling bounds, J. Cosmol. Astropart. Phys. 09 (2023) 009.
[42] M. J. Dolan, F. J. Hiskens, and R. R. Volkas, Constraining dark photons with self-consistent simulations of globular cluster stars, J. Cosmol. Astropart. Phys. 05 (2024) 099.
[43] F. X. Timmes and S. E. Woosley, The conductive propagation of nuclear flames. I. Degenerate C+O and O+NE+MG white dwarfs, Astrophys. J. **396**, 649 (1992).
[44] F. X. Timmes, Physical properties of laminar helium deflagrations, Astrophys. J. **528**, 913 (2000).
[45] J. Bramante, A. Delgado, and A. Martin, Multiscatter stellar capture of dark matter, Phys. Rev. D **96**, 063002 (2017).

[46] J. F. Acevedo and J. Bramante, Supernovae sparked by dark matter in white dwarfs, Phys. Rev. D **100**, 043020 (2019).
[47] S. Mashchenko and A. Sills, Globular clusters with dark matter halos. 1. Initial relaxation, Astrophys. J. **619**, 243 (2005).
[48] B. Moore, J. Diemand, P. Madau, M. Zemp, and J. Stadel, Globular clusters, satellite galaxies and stellar haloes from early dark matter peaks, Mon. Not. R. Astron. Soc. **368**, 563 (2006).
[49] T. R. Saitoh, J. Koda, T. Okamoto, K. Wada, and A. Habe, Tidal disruption of dark matter halos around proto-globular clusters, Astrophys. J. **640**, 22 (2006).
[50] B. F. Griffen, M. J. Drinkwater, P. A. Thomas, J. C. Helly, and K. A. Pimbblet, Globular cluster formation within the aquarius simulation, Mon. Not. R. Astron. Soc. **405**, 375 (2010).
[51] B. Willman and J. Strader, "Galaxy," defined, Astron. J. **144**, 76 (2012).
[52] E. J. Tollerud, J. S. Bullock, G. J. Graves, and J. Wolf, From galaxy clusters to ultra-faint dwarf spheroidals: A fundamental curve connecting dispersion-supported galaxies to their dark matter halos, Astrophys. J. **726**, 108 (2011).
[53] P. Creasey, L. V. Sales, E. W. Peng, and O. Sameie, Globular clusters formed within dark haloes I: Present-day abundance, distribution, and kinematics, Mon. Not. R. Astron. Soc. **482**, 219 (2019).
[54] P. Madau, A. Lupi, J. Diemand, A. Burkert, and D. N. C. Lin, Globular cluster formation from colliding substructure, arXiv:1905.08951.
[55] E. Vitral and P. Boldrini, Properties of globular clusters formed in dark matter mini-halos, Astron. Astrophys. **667**, A112 (2022).
[56] R. Garani, N. Raj, and J. Reynoso-Cordova, Could compact stars in globular clusters constrain dark matter?, J. Cosmol. Astropart. Phys. 07 (2023) 038.
[57] R. H. Helm, Inelastic and elastic scattering of 187-MeV electrons from selected even-even nuclei, Phys. Rev. **104**, 1466 (1956).
[58] N. Itoh, H. Hayashi, A. Nishikawa, and Y. Kohyama, Neutrino energy loss in stellar interiors. VII. Pair, photo-, plasma, bremsstrahlung, and recombination neutrino processes, Astrophys. J. **102**, 411 (1996).
[59] D. G. Yakovlev and V. A. Urpin, Thermal and electrical conductivity in white dwarfs and neutron stars, Sov. Astron. **24**, 303 (1980).
[60] M. Lampe, Transport coefficients of degenerate plasma, Phys. Rev. **170**, 306 (1968).
[61] V. A. Urpin and D. G. Yakovlev, Thermal conductivity due to collisions between electrons in a degenerate relativistic electron gas, Sov. Astron. **24**, 126 (1980).
[62] M. J. Harris, W. A. Fowler, G. R. Caughlan, and B. A. Zimmerman, Thermonuclear reaction rates, III, Annu. Rev. Astron. Astrophys. **21**, 165 (1983).
[63] Data reference.
[64] S. L. Shapiro and S. A. Teukolsky, Black holes, white dwarfs, and neutron stars: The physics of compact objects, 10.1002/9783527617661 (1983).
[65] H.-Y. Chiu, *Stellar Physics* (Blaisdell, New York, 1968), Vol. 1.
[66] J. R. Buchler and W. R. Yueh, Compton scattering opacities in a partially degenerate electron plasma at high temperatures, Astrophys. J. **210**, 440 (1976).
[67] T. A. Weaver, G. B. Zimmerman, and S. E. Woosley, Presupernova evolution of massive stars, Astrophys. J. **225**, 1021 (1978).
[68] B. Paczynski, Models of x-ray bursters with radius expansion, Astrophys. J. **267**, 315 (1983).
[69] J. Poutanen, Rosseland and flux mean opacities for Compton scattering, Astrophys. J. **835**, 119 (2017).
[70] N. Itoh, M. Nakagawa, and Y. Kohyama, Relativistic free-free opacity for a high-temperature stellar plasma, Astrophys. J. **294**, 17 (1985).
[71] W. J. Karzas and R. Latter, Electron radiative transitions in a Coulomb field, Astrophys. J. Suppl. Ser. **6**, 167 (1961).
[72] P. S. Shternin and D. G. Yakovlev, Electron thermal conductivity owing to collisions between degenerate electrons, Phys. Rev. D **74**, 043004 (2006).
[73] S. Cassisi, A. Y. Potekhin, A. Pietrinferni, M. Catelan, and M. Salaris, Updated electron-conduction opacities: The impact on low-mass stellar models, Astrophys. J. **661**, 1094 (2007).